

Magma Redox Geochemistry

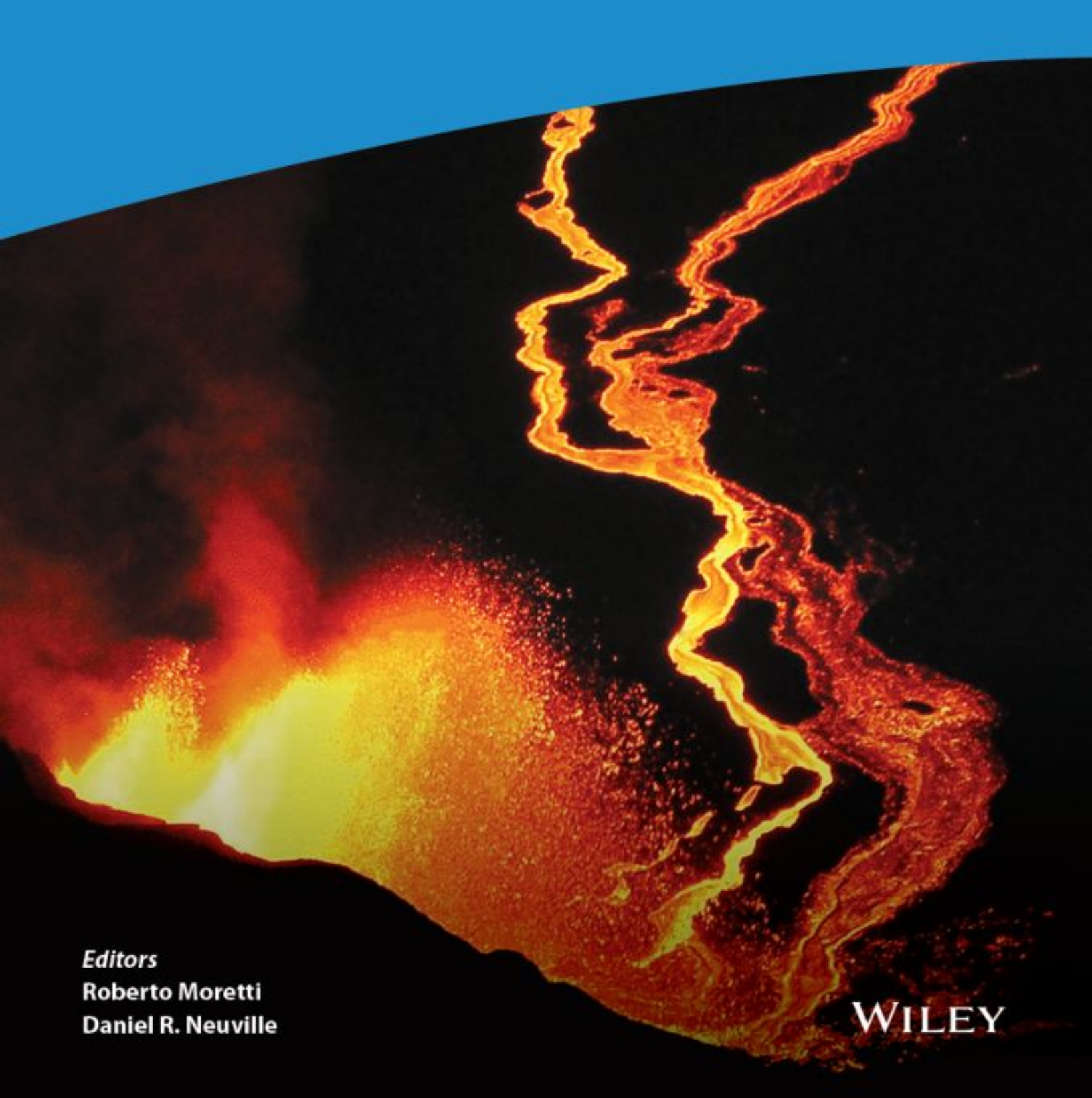


Table of Contents

Cover
<u>Series Page</u>
<u>Title Page</u>
<u>Copyright Page</u>
<u>List of Contributors</u>
<u>Preface</u>
1 Redox Equilibria
1.1. GENERAL ASPECTS AND RATIONALE
1.2. OXYGEN FUGACITY: THE CENTRALITY OF AN ELUSIVE PARAMETER
1.3. CONCLUDING REMARKS AND PERSPECTIVES
<u>ACKNOWLEDGMENTS</u>
<u>REFERENCES</u>
Part I: Redox from the Earth's Accretion to Global
Geodynamics
2 Redox Processes Before, During, and After Earth's Accretion Affecting the Deep Carbon Cycle 2.1. THE REDOX STATE OF PLANETARY
INTERIORS AND THE SPECIATION OF CARBON IN THE EARTH
2.2. OXIDATION STATE OF EARTH'S BUILDING BLOCKS AND EARLY DIFFERENTIATION
2.3. MANTLE OXIDATION STATE OVER TIME AND ITS EFFECT ON THE C-O-H VOLATILE SPECIATION

2.4. THE MANTLE GREAT OXIDATION EVENT:
FACT OR ARTEFACT?
<u>ACKNOWLEDGMENTS</u>
<u>REFERENCES</u>
3 Oxygen Fugacity Across Tectonic Settings
3.1. INTRODUCTION
3.2. SAMPLE SELECTION, METHODOLOGY, AND DESIGN OF THIS STUDY
3.3. RESULTS
3.4. DISCUSSION
3.5. CONCLUSIONS AND FUTURE
<u>DIRECTIONS</u>
<u>ACKNOWLEDGMENTS</u>
METHODS APPENDIX
<u>REFERENCES</u>
4 Redox Variables and Mechanisms in Subduction
<u>Magmatism and Volcanism</u>
4.1. INTRODUCTION
4.2. REDOX VARIABLES
4.3. MECHANISMS
4.4. DISCUSSION
<u>ACKNOWLEDGMENTS</u>
TIONITO WILLDONIENTO
REFERENCES
REFERENCES
REFERENCES 5 Redox Melting in the Mantle
REFERENCES 5 Redox Melting in the Mantle 5.1. INTRODUCTION
REFERENCES 5 Redox Melting in the Mantle 5.1. INTRODUCTION 5.2. MANTLE MELTING WITH VOLATILE

5.5. THE OXIDATION STATE IN THE MANTLE
LITHOSPHERE, ASTHENOSPHERE, AND
SUBDUCTION ZONES

5.6. DISCUSSION

5.7. CLOSING COMMENTS

ACKNOWLEDGMENTS

REFERENCES

<u>Part II: Redox at Work: From Magma Sources to</u> Volcanic Phenomena

6 Ionic Syntax and Equilibrium Approach to Redox Exchanges in Melts: Basic Concepts and the Case of Iron and Sulfur in Degassing Magmas

6.1. INTRODUCTION

6.2. IONIC SYNTAX, SPECIATION STATE AND THE MELT/GLASS NETWORK: STATE OF THE ART AND CONCEPTUAL FRAMEWORK

6.3. REDOX EVOLUTION AND MAGMATIC DEGASSING

6.4. DISCUSSION

6.5. CONCLUSIONS

CODE AVAILABILITY

ACKNOWLEDGMENTS

REFERENCES

7 The Petrological Consequences of the Estimated Oxidation State of Primitive MORB Glass

7.1. INTRODUCTION

7.2. MODELING METHODS AND SAMPLE SELECTION

7.3. RESULTS

7.4. SUMMARY AND PROSPECTS

ACKNOWLEDGMENTS
<u>REFERENCES</u>

8 Oxygen Content, Oxygen Fugacity, the Oxidation State of Iron, and Mid-Ocean Ridge Basalts

8.1. OXYGEN CONTENT, OXYGEN FUGACITY, AND THE OXIDATION STATE OF IRON

8.2. MID-OCEAN RIDGE BASALTS

<u>ACKNOWLEDGMENTS</u>

REFERENCES

9 Chromium Redox Systematics in Basaltic Liquids and Olivine

9.1. INTRODUCTION

9.2. MEASURING C_R VALENCE IN GEOLOGICMATERIALS WITH C_R -K EDGE XANES SPECTROSCOPY

9.3. C_R-REDOX SYSTEMATICS IN
SILICATELIQUIDS: WHAT WE KNOW AND
DON'T KNOW

9.4. C_R-VALENCE SYSTEMATICS
INEQUILIBRIUM LIQUID-OLIVINE PAIRS

9.5. CONCLUDING REMARKS

<u>ACKNOWLEDGMENTS</u>

REFERENCES

10 The Thermodynamic Controls on Sulfide Saturation in Silicate Melts with Application to Ocean Floor Basalts

10.1. INTRODUCTION

10.2. SULFIDE CAPACITY

10.3. THE THERMODYNAMIC MEANING OF THE SULFIDE CAPACITY

10.4. A NEW PARAMETERIZATION OF
SULFIDE CAPACITY FOR BASALTIC MELTS
10.5. SULFIDE CONTENT AT SULFIDE
SATURATION (SCSS)
10.6. APPLICATION TO MID-OCEAN RIDGE
AND SIMILAR BASALTS
10.7. THE SULFUR FUGACITY (fS ₂) OF
OCEAN FLOOR BASALTS
10.8. CONCLUSIONS
<u>ACKNOWLEDGMENTS</u>
<u>REFERENCES</u>
11 Redox State of Volatiles and Their Relationships
with Iron in Silicate Melts
11.1. INTRODUCTION
11.2. WATER CONCENTRATION IN MELT AND
ITS EFFECT ON REDOX
11.3. THE SULFUR SPECIES AND THE REDOX
(FE ³⁺ /∑FE Ratio) OF SILICATE MELTS
11.4. NATURAL SYSTEMS: MAGMA
DEGASSING AND REDOX
11.5. CONCLUDING REMARKS
<u>ACKNOWLEDGMENTS</u>
REFERENCES
12 Iron in Silicate Glasses and Melts
12.1. INTRODUCTION
12.2. IRON DISTRIBUTION IN THE
DIFFERENT TERRESTRIAL ENVELOPES
12.3. REDOX EQUILIBRIUM IN MELTS
12.4. PHYSICAL PROPERTIES: HIGHLIGHTS
ON DENSITY AND VISCOSITY

12.5. INFLUENCES ON CRYSTALLIZATION AND DEGASSING IN MAGMATIC SYSTEMS 12.6. CONCLUDING REMARKS **ACKNOWLEDGMENTS** REFERENCES Part III: Tools and Techniques to Characterize the Redox and its Effect on Isotope Partitioning 13 How to Measure the Oxidation State of Multivalent Elements in Minerals, Glasses, and Melts? 13.1. INTRODUCTION 13.2. WET-CHEMICAL ANALYSES 13.3. ELECTRONIC MICROPROBE 13.4. MÖSSBAUER SPECTROSCOPY 13.5. OPTICAL ABSORPTION SPECTROSCOPY 13.6. X-RAY ABSORPTION SPECTROSCOPY 13.7. RAMAN SPECTROSCOPY 13.8. IN SITU REDOX DETERMINATION AT HIGH TEMPERATURE OR AT HIGH PRESSURE 13.9. CONCLUSION **ACKNOWLEDGMENTS** REFERENCES 14 Oxidation State, Coordination, and Covalency Controls on Iron Isotopic Fractionation in Earth's Mantle and Crust 14.1. INTRODUCTION

14.2. THEORY: EQUILIBRIUM ISOTOPIC FRACTIONATION FROM VIBRATIONAL

PROPERTIES

14.3. CALCULATION OF VIBRATIONAL
<u>PROPERTIES</u>
14.4. IRON ISOTOPE STUDIES BASED ON
NRIXS OR DFT
14.5. COMPARISON OF EQUILIBRIUM
FRACTIONATION FACTORS DERIVED FROM
<u>VARIOUS TECHNIQUES</u>
14.6. PARAMETERS CONTROLLING
EQUILIBRIUM FRACTIONATION FACTORS
14.7. SELECTED APPLICATIONS TO THE
<u>INTERPRETATION OF IRON ISOTOPIC</u> VARIATIONS IN IGNEOUS ROCKS
14.8. CONCLUSIONS AND PERSPECTIVES
<u>ACKNOWLEDGMENTS</u>
<u>REFERENCES</u>
15 The Role of Redox Processes in Determining the
<u>Iron Isotope Compositions of Minerals, Melts, and</u> Fluids
15.1. INTRODUCTION
15.2. PRINCIPLES AND NOMENCLATURE
15.3. METHODS FOR THE CALIBRATION OF IRON ISOTOPE FRACTIONATION FACTORS
15.4. FUNDAMENTAL CONTROLS ON ISOTOPIC FRACTIONATION BETWEEN
MINERALS, MELTS, AND FLUIDS
15.5. EFFECT OF REDOX PROCESSES IN
INFLUENCING IRON ISOTOPE
FRACTIONATION IN NATURAL SYSTEMS
15.6. CONCLUSION
<u>ACKNOWLEDGMENTS</u>
REFERENCES

16 Zinc and Copper Isotopes as Tracers of Redox Processes
16.1. INTRODUCTION
16.2. THE DETERMINATION OF CU AND ZN ISOTOPE RATIOS
16.3. THEORETICAL AND EXPERIMENTAL
CONSTRAINTS ON CU AND ZN ISOTOPE BEHAVIOR IN RELATION TO REDOX
PROCESSES
16.4. APPLICATION OF CU AND ZN TO TRACE REDOX PROCESSES IN NATURAL SYSTEMS
16.5. SUMMARY AND CONCLUSIONS
<u>ACKNOWLEDGMENTS</u>
<u>REFERENCES</u>
17 Mineral-Melt Partitioning of Redox-Sensitive Elements
17.1. INTRODUCTION
17.2. THEORETICAL BACKGROUND
17.3. TRANSITION METALS (Fe, Cr, Ti, V)
17.4. RARE EARTHS (Ce, Eu)
<u>17.5. URANIUM (U)</u>
17.6. SIDEROPHILE ELEMENTS (Mo, W, Re, Pt GROUP ELEMENTS)
17.7. CONCLUDING REMARKS
<u>ACKNOWLEDGMENTS</u>
<u>REFERENCES</u>
18 Titanomagnetite - Silicate Melt Oxybarometry
18.1. INTRODUCTION
18.2. OXYBAROMETERS RELATED TO TITANOMAGNETITE

<u>18.3.</u>	<u>OXYBA</u>	<u>ROMETERS</u>	<u>S BASED</u>	<u>ON MINER</u>	AL
<u>EQU</u>	ILIBRIA	INVOLVIN	<u>G TITAN</u>	<u>OMAGNETI</u>	ГΕ

18.4. OXYBAROMETERS BASED ON ELEMENT PARTITIONING BETWEEN

TITANOMAGNETITE AND SILICATE MELT

18.5. APPLICATION OF TITANOMAGNETITE-BASED OXYBAROMETERS TO NATURAL

SILICIC ROCKS

18.6. CONCLUSIONS

ACKNOWLEDGMENTS

REFERENCES

SUPPLEMENTARY REFERENCES

19 The Redox Behavior of Rare Earth Elements

19.1. INTRODUCTION

19.2. GEOCHEMISTRY OF RARE EARTH ELEMENTS

19.3. MULTIVALENT RARE EARTH ELEMENTS

19.4. CONCLUSIONS AND PERSPECTIVES

ACKNOWLEDGMENTS

REFERENCES

<u>Index</u>

End User License Agreement

List of Tables

Chapter 3

Table 3.1 Results and Method Summary.

<u>Table A1 Major element criteria for "terrestrial"</u> <u>lavas between QFM -3 and ...</u> Table A2 Standard error (σ_{est}) of three fO_2 parameterizations.

Chapter 8

<u>Table 8.1 The percentage of O in different forms, or condensed by various re...</u>

Chapter 10

Table 10.1 Experimental studies used in parameterizing the sulfide content ...

<u>Table 10.2 Sulfur analyses in natural OFB glass</u> <u>VG2 (USNM 111240/52) by ele...</u>

Table 10.3 SCSS experiments in Re capsules at 1400°C, 1.5 GPa using the sta...

<u>Table 10.4 SCSS model sensitivities (anhydrous model).</u>

Chapter 12

Table 12.1 Example of optical basicity Λ of common network formers and modi...

Table 12.2 Viscosity data of DiFe0, DiFe6, DiFe12, and DiFe18 diopside melt...

Chapter 13

<u>Table 13.1 Fe and Mn crystalline compounds</u> reported in Fig. 13.6. Experimen...

<u>Table 13.2 Summarize of analytical techniques and their advantages.</u>

Chapter 14

<u>Table 14.1 Iron</u> β -factors ($^{56/54}$ Fe) derived from first-principles calcu...

List of Illustrations

Chapter 1

Figure 1.1 E-pH diagram reporting the stability of water at T = 25°C and P = ...

<u>Figure 1.2 The E-pH (Pourbaix) diagram for the Fe-S-H₂O system at 25°C at 1 ...</u>

<u>Figure 1.3 Limit of equilibrium potential-pO²⁻</u> graphs in molten alkali...

<u>Figure 1.4 Log fO₂ - Ph diagrams for 290°C (left panel) and 145°C (right pan...</u>

Figure 1.5 (a) Ellingham diagram for the main components of the melt/slag (s...

<u>Figure 1.6 Common solid oxygen buffers used in petrology and geochemistry. T...</u>

<u>Figure 1.7 Two-redox potential fO₂-fS₂ diagram.</u>
The conformation of stabilit...

Chapter 2

Figure 2.1 Range of oxygen fugacity estimates for Solar Nebula, achondrites,...

<u>Figure 2.2 LogfO₂ (normalized to the FMQ buffer)</u> calculated for mantle perid...

<u>Figure 2.3 (a) V/Sc and (B) calculated LogfO₂</u> (normalized to the FMQ buffer)...

Chapter 3

<u>Figure 3.1 Locations of samples compiled in this study as a function of tect...</u>

Figure 3.2 Distribution of fO_2 recorded by volcanics globally in different t...

<u>Figure 3.3 Distribution of fO₂ recorded by mantle lithologies (peridotites a...</u>

Figure 3.4 V/Yb ratios of ridge (gray "+" symbols, Gale et al., 2013), back-...

<u>Figure 3.5 Progressive degassing of a C-O-H-S vapor in ridge, arc, and plume...</u>

Figure 3.6 Magmatic oxygen fugacity as recorded by volcanics for samples in ...

<u>Figure A1 Temperatures and values of fO₂ from the model of Ghiorso and Evans...</u>

<u>Figure A2 XANES spectra of MORB glass VG3385</u> with spectra of mid-ocean ridge...

<u>Figure A3 The measured experimental furnace fO_2 in log units relative to the...</u>

Chapter 4

<u>Figure 4.1 Positions of redox buffers at 1 bar. From Frost, (1991) unless ot...</u>

<u>Figure 4.2 Conceptual model of subduction zone cycling.</u>

<u>Figure 4.3 Location of volcanic arcs and spreading</u> <u>ridges mentioned in the t...</u>

Chapter 5

Figure 5.1 (a) Solidus curves for peridotite in dry conditions (black line) ...

Figure 5.2 Two depictions of the reduced and oxidized fluid realms for COH f...

<u>Figure 5.3 Illustration of the fO₂ levels at which</u> <u>HRM and CRM occur, relate...</u>

<u>Figure 5.4 Illustration of pressure effects on the</u> extent of redox fractiona...

<u>Figure 5.5 Ranges of redox states found in various geodynamic settings and i...</u>

<u>Figure 5.6 Illustration of redox fronts that develop</u> <u>between lithosphere and...</u>

<u>Figure 5.7 Comparison of likely widely applicable</u> <u>peridotite solidi in Phane...</u>

Chapter 6

Figure 6.1 (a) Oxidized/reduced iron (log-form) for simple binaries at 1400°...

Figure 6.2 (a) Comparison of Paul and Douglas (1965) data with those of Tang...

Figure 6.3 (a) S^{VI}/S_{tot} from empirical formulations available in the literat...

<u>Figure 6.4 Mutual interaction of iron and sulfur redox couples in dry and hy...</u>

<u>Figure 6.5 Patterns of sulfur release and their effect on melt sulfur distri...</u>

<u>Figure 6.6 Covariation of sulfate and sulfide</u> contents in andesitic to rhyol...

Figure 6.7 (a) Covariation of sulfate and sulfide fractions in melt inclusio...

Figure 6.8 (a) Plot of $logK_{15}$ vs $logfO_2$, showing the nearly negligible effec...

<u>Figure 6.9 (a) Melt sulfate/sulfide ratios vs.</u> <u>dissolved water contents from...</u>

Chapter 7

<u>Figure 7.1 Histograms of measurements of the Fe²⁺/Fe^T ratio in global survey...</u>

<u>Figure 7.2 A simple model of olivine-liquid</u> <u>equilibria and FeO-MgO systemati...</u>

Figure 7.3 PRIMELT3 outputs from calculation of primary magma parental to th...

<u>Figure 7.4 PRIMELT3 prediction for the Mg# of the liquidus olivine that firs...</u>

<u>Figure 7.5 PRIMELT3 predictions for the Mg# of the liquidus olivine that fir...</u>

<u>Figure 7.6 Predictions of the pMELTS model of oceanic crustal production for...</u>

<u>Figure 7.7 rhyoliteMELTS calculations showing the fraction of original liqui...</u>

Chapter 8

<u>Figure 8.1 Histogram of the log(abundance) of 78 elements (M; bin size 0.5) ...</u>

Figure 8.2 $\log(Fe^{3+}/Fe^{2+})$ as a function of fO_2 , relative to the quartz-fayal...

Figure 8.3 Fe³⁺/ Σ Fe as a function of fO_2 , relative to the QFM buffer, predic...

<u>Figure 8.4 (a) log Fe₂O₃ (in wt%) of MORB glasses</u> determined by Berry et al....

Chapter 9

<u>Figure 9.1 XANES spectra from Cr²⁺ and Cr³⁺ standard glasses. There are seve...</u>

<u>Figure 9.2 Adapted from Bell et al. (2017);</u> illustrates how the crystallogra...

Figure 9.3 $Cr^{2+}/\Sigma Cr$ ratios plotted vs. experimental fO_2 from Roedder and Rey...

Figure 9.4 Contains plots the XANES measured the $Cr^{2+}/\Sigma Cr$ ratios from quench...

<u>Figure 9.5 Cr partitioning data compiled from several studies plotted vs. ex...</u>

Figure 9.6 XANES measured Cr²⁺/\(\sum_{Cr}\) values of a set of experimentally grown o...

Chapter 10

Figure 10.1 Comparison between values of $A_M^{S^2}$ from O'Neill and Mavrogenes (2002...

Figure 10.2 The relationship between $S^{6+}/\Sigma S$ and $Fe^{3+}/\Sigma Fe$, estimated by combi...

Figure 10.3 (a) Observed values of the sulfide capacity, C_{S^2} , at 1400°C of sil...

<u>Figure 10.4 Comparison between measured values</u> of the activity coefficient o...

<u>Figure 10.5 The oxygen contents as the component</u> <u>FeO in sulfide mattes coexi...</u>

Figure 10.6 The effect of pressure on the SCSS, comparing Equation 10.43 of ...

<u>Figure 10.7 SCSS for a binary compositional join</u> between FeO-free "matrix" a...

Figure 10.8 The effect of H_2O on SCSS. Data from Moune et al. (2009) at 1045...

Figure 10.9 Sulfur saturation in ocean floor basaltic (OFB) glasses from Jen...

<u>Figure 10.10 The difference between [S]_{obs} and the calculated SCSS from the ...</u>

<u>Figure 10.11 Calculated atomic Ni/Fe (a) and Cu/Fe (b) in sulfide liquid in ...</u>

Figure 10.12 Comparison with the SCSS model of Smythe et al. (2017). (a) Cal...

Figure 10.13 (a) Reproducibility of S analyses in basaltic glasses: a compar...

Figure 10.14 Comparison of model $[S]_{SCSS}$ with $[S]_{obs}$ for Macquarie Island ba...

Figure 10.15 Comparison between model [S]_{SCSS} and [S]_{obs} for two sets of gla...

<u>Figure 10.16 Olivine-hosted melt inclusions from Le Voyer et al. (2017). (a)...</u>

<u>Figure 10.17 Ni and Cu abundances in ocean floor basaltic (OFB) glasses vers...</u>

Figure 10.18 Calculated [S]_{SCSS} vs. [S]_{obs} for olivine-hosted melt inclusion...

<u>Figure 10.19 (a) log₁₀ fS₂ and (b) log₁₀ fSO₂ calculated for 35 sulfide-satu...</u>

Chapter 11

<u>Figure 11.1 Isobaric calculations of H₂O and CO₂</u> contents in Basaltic melt a...

Figure 11.2 Variation of the log <u>fO</u>₂ values as a <u>function of the temperature...</u>

<u>Figure 11.3 Experimentally determined S solubility</u> data of basaltic melts as...

<u>Figure 11.4 Sulfur valence state at fO_2 , expressed relative to FMQ. Figure m...</u>

<u>Figure 11.5 Influence of oxygen fugacity on the partitioning of sulfur betwe...</u>

Chapter 12

<u>Figure 12.1 Examples of iron concentration ([FeO] equivalent) in various ign...</u>

Figure 12.2 Variation of the Fe³⁺/Fe^{TOT} (Fe^{TOT} = $Fe^{2+} + Fe^{3+}$) redox ratio as...

<u>Figure 12.3 Iron oxidation state in K₂O-Al₂O₃-SiO₂-FeO melts at 1673 K in ai...</u>

<u>Figure 12.4 Examples of compositional effects on</u> the oxidation state of iron...

<u>Figure 12.5 Viscosity of (a) anorthite-diopside (An-Di) eutectic melt as a f...</u>

Figure 12.6 Viscosity of SiO_2 , $NaAlSi_3O_8$ and $NaFeSi_3O_8$ melts.

<u>Figure 12.7 Isothermal viscosity as a function of the oxidation state of iro...</u>

<u>Figure 12.8 Effects of the crystal (a) and water (b) contents on the viscosi...</u>

Figure 12.9 Viscosity, crystallinity, and oxidation state of andesite and ba...

Chapter 13

<u>Figure 13.1 Mössbauer spectra of an Fe-bearing</u> diopside glass prepared at 15...

<u>Figure 13.2 Example of Optical Absorption spectra</u> <u>of glasses containing diff...</u>

<u>Figure 13.3 Optical absorption spectrum, in the range 4000–28500 cm⁻¹,...</u>

<u>Figure 13.4 Optical Absorption spectrum of a V-doped sodium aluminosilicate ...</u>

<u>Figure 13.5 Energy scaled K-edge XAS spectrum of vanadium in divanadium trio...</u>

<u>Figure 13.6 XANES spectra of first- row multivalent</u> transition metal oxides ...

<u>Figure 13.7 K-edge XANES spectra of Mn (a) and Fe (b) crystalline compounds ...</u>

<u>Figure 13.8 Cerium L_{III}-edge XANES spectra for two Ce crystalline materials ...</u>

Figure 13.9 Schematic drawing of a lava, and XAS spectra at the Fe K-edge an...

Figure 13.10 Raman spectrum of an iron-free pyroxene glass (CaO-SiO₂-Na₂O-Mg...

<u>Figure 13.11 Raman spectra at room temperature</u> <u>for a series of iron-pyroxene...</u>

Figure 13.12 **a,b**: Deconvolution of the 0.09 and 0.99 Raman spectra (based on ...

Figure 13.13 Comparison of iron ratios analyzed by different techniques, wet...

Figure 13.14 (a) Evolution of the normalized XANES spectra at the Fe K-edge a...

<u>Figure 13.15 Fe³⁺/Fe_{Tot} redox as different temperatures, 412, 618, 710 °C fr...</u>

Chapter 14

Figure 14.1 Generic example of the temperature dependence of the β -fact...

<u>Figure 14.2 Relative departure (numbers on the curves) from Equation 14.8 in...</u>

Figure 14.3 Iron β-factors ($\frac{56}{54}$ Fe) at 298 K as a function of the iron...

Figure 14.4 Temperature dependence of iron β-factors ($^{56/54}$ Fe) for mine...

Figure 14.5 Iron β-factors ($\frac{56}{54}$ Fe) at 298 K as a function of the aver...

<u>Figure 14.6 XANES centroid energy (left) and mean</u> <u>force constant of iron mea...</u>

Chapter 15

Figure 15.1 After Sossi and O'Neill (2017). Dependence of the calculated for...

Figure 15.2 Iron-oxygen force constants in spinel group minerals (after Rosk...

Figure 15.3 After Dauphas et al. (2014). Mean force constants of Fe-O bonds ...

Figure 15.4 After Liu et al. (2017). Force constants (N/m) of iron bonds in ...

Figure 15.5 After Fujii et al. 2014. Temperature dependence of the $10^3 \ln \beta^{56/}$...

Figure 15.6 Melting models from Sossi & O'Neill (2017) (see Equations 15.21-...

Figure 15.7 After Sossi and O'Neill (2017). Iron isotope composition of mafi...

Figure 15.8 After Foden et al. (2018). δ^{57} Fe_(IRMM-14) vs. Slab Thermal...

<u>Figure 15.9 After Heimann et al. 2008. An early compilation of iron isotope ...</u>

Figure 15.10 δ^{57} Fe of whole rocks against their Mg#, characterizing the chan...

<u>Figure 15.11 After Du et al. 2017. Compilation of Fe isotope mineral composi...</u>

Figure 15.12 After Debret et al. (2016). Increase in δ^{56} Fe and decrease of F...

Chapter 16

<u>Figure 16.1 A periodic stable showing traditional</u> and selected non-tradition...

<u>Figure 16.2 The temperature dependent of ln β or isotopic enrichment factor,...</u>

<u>Figure 16.3 A Rayleigh fractionation model</u> <u>summarizing the key experimental ...</u>

<u>Figure 16.4 Temperature dependence of ln β</u> <u>between different Zn-S and Zn-C s...</u>

Figure 16.5 The effect of and temperature $log fO_2$ on the speciation of Cu wi...

Chapter 17

Figure 17.1 (a) Schematic illustration of lattice strain parameters D_0, r_0, \dots

<u>Figure 17.2 Relative oxygen fugacity conditions (in log units relative to FM...</u>

<u>Figure 17.3 Mineral/melt partitioning of transition</u> metals as a function of ...

<u>Figure 17.4 Comparison of Cr olivine(Fo₁₀₀)/melt</u> partitioning coefficients o...

<u>Figure 17.5 Zircon/melt partition coefficients for</u> REE elements determined e...

<u>Figure 17.6 Mineral/melt partitioning of redox-</u> <u>sensitive rare earth elements...</u>

<u>Figure 17.7 Mineral/melt partitioning of U as a function of oxygen fugacity ...</u>

<u>Figure 17.8 Mineral/melt partitioning of siderophile elements (Mo, W, and Re...</u>

Chapter 18

Fig. S1 Summary of commonly applied oxygen fugacity buffers and their positi...

Fig. 18.1 Graphical representation of the magnetite-ilmenite oxybarometer/th...

Fig. 18.2 Estimated proportions of V^{3+} , V^{4+} , and V^{5+} in a ferrobasaltic melt...

Fig. 18.3 Results of titanomagnetite-melt vanadium partitioning experiments ...

Fig. 18.4 (a) Iron solubility in rhyolite melts as a function of alumina sat...

Fig. 18.5 Performance of FeTiMM on experimental samples. Oxygen fugacities (...

Fig. 18.6 (a) Comparison of fO_2 values (reported in log units relative to th...

Fig. 18.7 The principle of the equilibrium test between magnetite and melt p...

Chapter 19

Figure 19.1 (a) Plot of ionic radius (data from Shannon, 1976) vs. ionic cha...

Figure 19.2 Ionic radii for six-fold coordinated REE³⁺. (Radius values from ...

Figure 19.3 (a) Mineral/melt REE partition coefficients for plagioclase (Plg...

Figure 19.4 Experimental data from Drake (1975) show that the partitioning o...

Figure 19.5 $Eu^{2+}/(Eu^{2+} + Eu^{3+})$ redox fraction as determined by XANES vs. oxy...

Figure 19.6 Dependence of the Ce⁴⁺/Ce_{tot} redox ratio on alkali content, and ...

Figure 19.7 Parallel (VV) and cross-polarized (VH) Raman spectra (normalized...

<u>Figure 19.8 X-Ray Absorption Spectroscopy data at the Eu L_{III}-edge (left) an...</u>

Figure 19.9 (a) XAS spectra, normalized at the Fe K-edge, collected for the ...

Geophysical Monograph Series

217	Deep Earth: Physics and Chemistry of the Lower Mantle and Core <i>Hidenori Terasaki and Rebecca A. Fischer (Eds.)</i>
218	Integrated Imaging of the Earth: Theory and Applications Max Moorkamp, Peter G. Lelievre, Niklas Linde, and Amir Khan (Eds.)
219	Plate Boundaries and Natural Hazards <i>Joao Duarte and Wouter Schellart (Eds.)</i>
220	Ionospheric Space Weather: Longitude and HemisphericDependences and Lower Atmosphere Forcing TimothyFuller-Rowell, Endawoke Yizengaw, Patricia H. Doherty, and Sunanda Basu (Eds.)
221	Terrestrial Water Cycle and Climate Change Natural andHuman-Induced Impacts Qiuhong Tang and Taikan Oki (Eds.)
222	Magnetosphere-Ionosphere Coupling in the Solar System Charles R. Chappell, Robert W. Schunk, Peter M. Banks, James L. Burch, and Richard M. Thorne (Eds.)
223	Natural Hazard Uncertainty Assessment: Modeling and Decision Support Karin Riley, Peter Webley, and Matthew Thompson (Eds.)
224	Hydrodynamics of Time-Periodic Groundwater Flow:Diffusion Waves in Porous Media Joe S. Depner and Todd C. Rasmussen (Auth.)
225	Active Global Seismology Ibrahim Cemen and Yucen

226	Climate Extremes Simon Wang (Ed.)
227	Fault Zone Dynamic Processes <i>Marion Thomas</i> (Ed.)
228	Flood Damage Survey and Assessment: New Insights fromResearch and Practice Daniela Molinari, Scira Menoni, and Francesco Ballio (Eds.)
229	Water-Energy-Food Nexus - Principles and Practices P. Abdul Salam, Sangam Shrestha, Vishnu Prasad Pandey, and Anil K Anal (Eds.)
230	Dawn-Dusk Asymmetries in Planetary PlasmaEnvironments Stein Haaland, Andrei Rounov, and Colin Forsyth (Eds.)
231	Bioenergy and Land Use Change Zhangcai Qin, Umakant Mishra, and Astley Hastings (Eds.)
232	Microstructural Geochronology: Planetary Records Downto Atom Scale Desmond Moser, Fernando Corfu, James Darling, Steven Reddy, and Kimberly Tait (Eds.)
233	Global Flood Hazard: Applications in Modeling, Mappingand Forecasting Guy Schumann, Paul D. Bates, Giuseppe T. Aronica, and Heiko Apel (Eds.)
234	Pre-Earthquake Processes: A Multidisciplinary Approach toEarthquake Prediction Studies Dimitar Ouzounov, Sergey Pulinets, Katsumi Hattori, and Patrick Taylor (Eds.)
235	Electric Currents in Geospace and Beyond Andreas Keiling, Octav Marghitu, and Michael Wheatland (Eds.)
236	Quantifying Uncertainty in Subsurface Systems Celine Scheidt, Lewis Li, and Jef Caers (Eds.)
237	Petroleum Engineering Moshood Sanni (Ed.)
238	Geological Carbon Storage: Subsurface Seals

and Caprock Integrity Stephanie Vialle, Jonathan Ajo-Franklin, and J. William Carey (Eds.) **239** Lithospheric Discontinuities Huaiyu Yuan and Barbara Romanowicz (Eds.) 240 Chemostratigraphy Across Major Chronological Eras Alcides N.Sial. Claudio Gaucher. Muthuvairavasamv Ramkumar, and Valderez Pinto Ferreira (Eds.) 241 Mathematical Geoenergy: Discovery, Depletion, and Renewal Paul Pukite, Dennis Coyne, and Daniel Challou (Eds.) 242 Ore Deposits: Origin, Exploration, and **Exploitation** Sophie Decree and Laurence Robb (Eds.) 243 Kuroshio Current: Physical, Biogeochemical andEcosystem Dynamics Takeyoshi Nagai, Hiroaki Saito, Koji Suzuki, and Motomitsu Takahashi (Eds.) 244 Geomagnetically Induced Currents from the Sun to the Power Grid Jennifer L. Gannon, Andrei Swidinsky, and Zhonghua Xu (Eds.) 245 Shale: Subsurface Science and Engineering Thomas Dewers, Jason Heath, and Marcelo Sánchez (Eds.) 246 Submarine Landslides: Subaqueous Mass TransportDeposits From Outcrops to Seismic **Profiles** Kei Ogata, Andrea Festa, and Gian Andrea Pini (Eds.) 247 Iceland: Tectonics, Volcanics, and Glacial **Features** *Tamie J. Jovanelly* **248** Dayside Magnetosphere Interactions *Qiuqang* Zong, Philippe Escoubet, David Sibeck, Guan Le, and Hui Zhang (Eds.)

- 249 Carbon in Earth's Interior Craig E. Manning, Jung-Fu Lin, and Wendy L. Mao (Eds.)
 250 Nitrogen Overload: Environmental
- 250 Nitrogen Overload: Environmental Degradation, Ramifications, and Economic Costs Brian G. Katz
- 251 Biogeochemical Cycles: Ecological Drivers and Environmental Impact Katerina Dontsova, Zsuzsanna Balogh-Brunstad, and Gaël Le Roux (Eds.)
- 252 Seismoelectric Exploration: Theory, Experiments, andApplications Niels Grobbe, André Revil, Zhenya Zhu, and Evert Slob (Eds.)
- 253 El Niño Southern Oscillation in a Changing Climate Michael J. McPhaden, Agus Santoso, and Wenju Cai (Eds.)
- **254** Dynamic Magma Evolution Francesco Vetere (Ed.)
- 255 Large Igneous Provinces: A Driver of GlobalEnvironmental and Biotic Changes
 Richard. E. Ernst, Alexander J. Dickson, and Andrey
 Bekker (Eds.)
- 256 Coastal Ecosystems in Transition: A Comparative Analysisof the Northern Adriatic and Chesapeake Bay Thomas C. Malone, Alenka Malej, and Jadran Faganeli (Eds.)
- 257 Hydrogeology, Chemical Weathering, and Soil Formation Allen Hunt, Markus Egli, and Boris Faybishenko (Eds.)
- **258** Solar Physics and Solar Wind Nour E. Raouafi and Angelos Vourlidas (Eds.)
- **259** Magnetospheres in the Solar System Romain Maggiolo, Nicolas André, Hiroshi Hasegawa, and Daniel T. Welling (Eds.)
- **260 Ionosphere Dynamics and Applications** *Chaosong*

	Huang and Gang Lu (Eds.)
261	Upper Atmosphere Dynamics and Energetics Wenbin Wang and Yongliang Zhang (Eds.)
262	Space Weather Effects and Applications <i>Anthea J. Coster, Philip J. Erickson, and Louis J. Lanzerotti (Eds.)</i>
263	Mantle Convection and Surface Expressions Hauke Marquardt, Maxim Ballmer, Sanne Cottaar, and Jasper Konter (Eds.)
264	Crustal Magmatic System Evolution: Anatomy, Architecture, and Physico-Chemical Processes Matteo Masotta, Christoph Beier, and Silvio Mollo (Eds.)
265	Global Drought and Flood Observation, Modeling, and Prediction Huan Wu, Dennis P. Lettenmaier, Qiuhong Tang, and Philip J. Ward (Eds.)
266	Magma Redox Geochemistry Roberto Moretti and Daniel R. Neuville (Eds.)

Magma Redox Geochemistry

Roberto Moretti Daniel R. Neuville Editors

This Work is a co-publication of the American Geophysical Union and John Wiley and Sons, Inc.



This edition first published 2022 © 2022 American Geophysical Union

All rights reserved. No part of this publication may be reproduced, stored in a retrieval system, or transmitted, in any form or by any means, electronic, mechanical, photocopying, recording or otherwise, except as permitted by law. Advice on how to obtain permission to reuse material from this title is available at http://www.wiley.com/go/permissions.

The right of Roberto Moretti and Daniel R. Neuville to be identified as the editor of this work has been asserted in accordance with law.

Published under the aegis of the AGU Publications Committee

Matthew Giampoala, Vice President, Publications Carol Frost, Chair, Publications Committee For details about the American Geophysical Union visit us at www.agu.org.

Registered Office

John Wiley & Sons, Inc., 111 River Street, Hoboken, NJ 07030, USA

Editorial Office

111 River Street, Hoboken, NJ 07030, USA

For details of our global editorial offices, customer services, and more information about Wiley products visit us at www.wiley.com.

Wiley also publishes its books in a variety of electronic formats and by print-ondemand. Some content that appears in standard print versions of this book may not be available in other formats.

Limit of Liability/Disclaimer of Warranty

While the publisher and authors have used their best efforts in preparing this work, they make no representations or warranties with respect to the accuracy or completeness of the contents of this work and specifically disclaim all warranties, including without limitation any implied warranties of merchantability or fitness for a particular purpose. No warranty may be created or extended by sales representatives, written sales materials or promotional statements for this work. The fact that an organization, website, or product is referred to in this work as a citation and/or potential source of further information does not mean that the publisher and authors endorse the information or services the organization, website, or product may provide or recommendations it may make. This work is sold with the understanding that the publisher is not engaged in rendering professional services. The advice and strategies contained herein may not be suitable for your situation. You should consult with a specialist where appropriate. Further, readers should be aware that websites listed in this work may have changed or disappeared between when this work was written and when it is read. Neither the publisher nor authors shall be liable for any loss of profit or any other commercial damages, including but not limited to special, incidental, consequential, or other damages.